iScience

CellPress
OPEN ACCESS

Article

adducin 1 is essential for the survival of erythroid precursors via regulating *p53* transcription in zebrafish

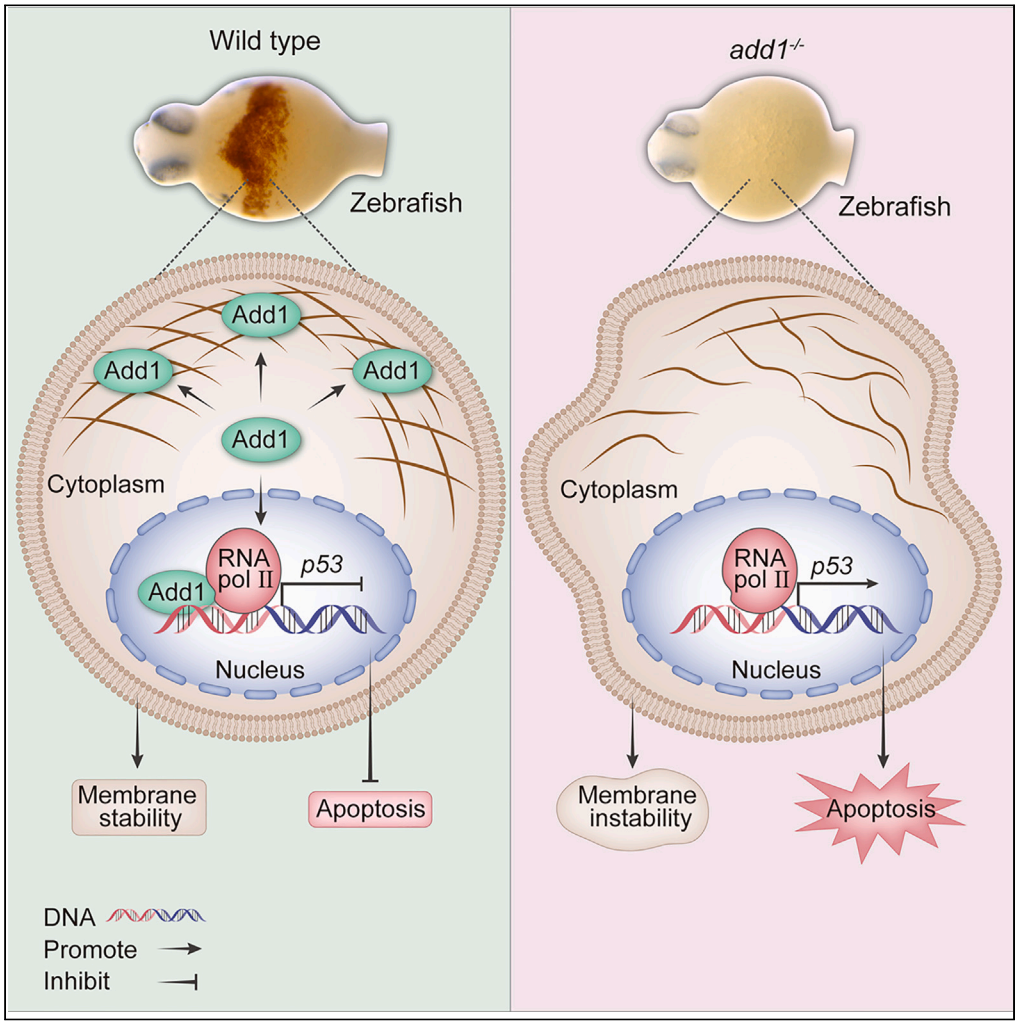

Shuyan Yang, Shanhu Cao, Xuebing Xu, ..., Ting Zhang, Li Wang, Shaoguang Sun

shuyanyang79@126.com (S.Y.)
lily_wang@yeah.net (L.W.)
sunshaoguang00@163.com (S.S.)

Highlights

Add1 is essential for primitive erythropoiesis and definitive hematopoiesis in zebrafish

The erythroblasts undergo apoptosis partially dependent on p53 due to *add1*-depletion

ADD1 downregulates p53 at the transcriptional level

Yang et al., iScience *26*, 107516
September 15, 2023
https://doi.org/10.1016/j.isci.2023.107516

iScience

CellPress
OPEN ACCESS

Article

adducin 1 is essential for the survival of erythroid precursors via regulating *p53* transcription in zebrafish

Shuyan Yang,[1,*] Shanhu Cao,[2] Xuebing Xu,[1,3] Quan Li,[4] Jianting Li,[5] Jin Guo,[1] Fang Wang,[1] Yihua Bao,[1] Zean Jiang,[2] Ting Zhang,[1] Li Wang,[1,*] and Shaoguang Sun[2,6,*]

SUMMARY

Adducin 1 (Add1) is known as a membrane cytoskeletal protein, but its nuclear function remains unclear. In this study, we generated *add1*-deficient zebrafish to investigate its role in hematopoiesis. Lack of *add1* impaired both primitive and definitive hematopoiesis, preventing healthy erythrocyte development. RNA sequencing revealed activation of the p53 pathway in *add1*-depleted erythroblast cells, leading to apoptosis at the 14-somites stage and 24 hpf. Interestingly, partial rescue of the anemic phenotype and apoptosis was observed with *p53* insufficiency. Mechanistically, ADD1 was found to regulate promoter activity. These findings demonstrate that Add1 plays a crucial role in zebrafish erythropoiesis, involving the p53-mediated apoptotic pathway, expanding its regulatory role beyond cytoskeletal functions.

INTRODUCTION

The Adducin (ADD) family proteins, namely ADD1, ADD2, and ADD3, are actin-binding proteins localized at actin-spectrin junctions, a strategic site for control of the stabilization of membrane cytoskeleton. It is expressed as heterotetramers in heterodimeric combinations with *ADD1/2* or *ADD1/3*.[1] There is a significant sequence, structural, and functional homology among ADDs.[2] In *Add1*-null mice, Add2 and Add3 proteins are undetectable,[3,4] indicating a predominant role of Add1 in stabilizing Add2 and Add3. *Add1*-null mice display growth retardation, compensated hemolytic anemia, and approximately 50% developed lethal communicating hydrocephalus accompanied by dilation of the ventricles.[3] Genetic variants of *ADD1* may disrupt the membrane skeleton and in turn influence a variety of physiological processes and manifests in diverse diseases, such as hypertension,[5,6] hemorrhagic stroke,[7] myocardial infarction,[8] atherosclerosis,[9] renal diseases,[10,11] and colorectal cancer.[12] However, the precise pathogenetic mechanisms of Add1/ADD1 involved need to be elucidated further.

Although ADDs function primarily as membrane cytoskeletal proteins, all the ADDs contain a highly conserved bipartite nuclear localization signal (NLS) at the carboxyl termini,[13,14] implying their special nuclear function. Compared to ADD2 and ADD3, ADD1 tends to localize in the nucleus and can interact with RNA polymerase II, zinc-finger protein 331(ZNF331),[15,16] or regulatory factor X1 (RFX1),[17] indicating a diversity of nuclear functional roles apart from maintaining cytoskeletal stability. However, whether ADD1 participates in hematopoiesis via regulating transcriptional levels of target genes remains unknown.

Zebrafish are very suitable for hematopoiesis development studies. Transient genetic manipulation by microinjection of mRNA or antisense morpholino oligonucleotides (MOs) provides convenient methods for functionally assessing genetic regulatory pathways without needing extended breeding strategies.[18] Zebrafish developmental hematopoiesis closely resembles mammalian hematopoiesis and is regulated by a conserved molecular pathway.[19] Many zebrafish mutants with hematopoiesis defects at various stages are identified in a large-scale chemical mutagenesis screen.[20] and several mutants model human hematopoiesis diseases.[21,22] Whereas, there is currently no *add1*-null zebrafish model, so it is valuable to create *add1* mutant zebrafish to elucidate the regulatory role of *add1* during hematopoiesis.

In this work, we obtained a zebrafish mutant with *add1*-deficient using Tol2 transposon-mediated gene trapping and found that loss of *add1* leads to defective assembly of erythrocyte membrane proteins,

[1]Beijing Municipal Key Laboratory of Child Development and Nutriomics, Capital Institute of Pediatrics, Beijing 100020, China

[2]Department of Biochemistry and Molecular Biology, Key Laboratory of Medical Biotechnology of Hebei Province, Cardiovascular Medical Science Center, Hebei Medical University, Shijiazhuang 050017, China

[3]Affiliated Hospital of Weifang Medical University, School of Clinical Medicine, Weifang Medical University, Weifang, China

[4]Beijing Institutes of Life Science Chinese Academy of Sciences, Beijing 100101, China

[5]Department of Biochemistry and Molecular Biology, Shanxi Medical University, Taiyuan 030001, China

[6]Lead contact

*Correspondence: shuyanyang79@126.com (S.Y.), lily_wang@yeah.net (L.W.), sunshaoguang00@163.com (S.S.)

https://doi.org/10.1016/j.isci.2023.107516

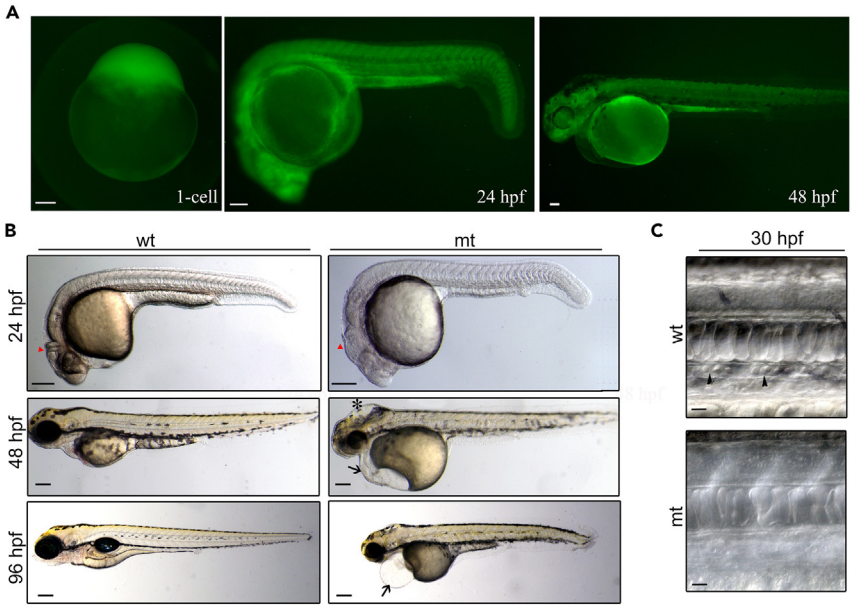

Figure 1. GFP expression pattern and phenotypes of *add1*$^{-/-}$ transgenic embryos

(A) Fluorescent images of *add1*$^{-/-}$ embryos. GFP was expressed maternally from the 1-cell stage and ubiquitously distributed along the whole body from 24 hpf to 48 hpf. Scale bars, 100 μm.

(B) Morphology of *add1*$^{-/-}$ mutant and sibling embryos. At 24 hpf, MHB was poorly developed in the homozygous mutant embryos (red triangle). Swelling of the hindbrain was observed in homozygous mutant embryos at 48 hpf (black star). Black arrow showed the trimmer head and smaller eyes in homozygous mutant embryos at 48 hpf. The mutant embryos developed edema at 96 hpf compared to siblings. Scale bars, 100 μm.

(C) Bright-field microscopy of blood cells in WT and mutant embryos at 30 hpf. Some blood cells could be observed in the caudal veins of siblings at 30 hpf (black arrowheads), whereas they were almost absent in the mutants. Scale bars, 10 μm.

impairment of erythrocyte maturation and defective definitive hematopoiesis. The mechanism was that *add1* deficiency activated the *p53*-mediated apoptotic pathway from the transcriptional level. Our findings provide a new nuclear functional role of *add1* apart from maintaining cytoskeletal stability.

RESULTS

add1$^{-/-}$ transgenic embryos express GFP ubiquitously and homozygous embryos are embryonic lethal

Using the Tol2 transposon-mediated gene tapping technique, we carried out a small-scale gene trap screen in zebrafish.[23] The Tol2-transposase mRNA was generated *in vitro*, then co-injected into zebrafish embryos at the one-cell stage together with a modified Tol2-based transposon trap vector called TSG that contained a splice acceptor and a promoterless GFP reporter.[20,24,25] We identified a mutant line named *add1*$^{-/-}$ after identifying the interrupted gene in our previous work. In this line, the embryos expressed green fluorescent protein (GFP) at the 1-cell stage (Figure 1A), suggesting that the trapped gene is maternally expressed. The expression pattern of GFP in this line is ubiquitous. Around 24 h postfertilization (hpf), the embryos can be classified into three groups according to the intensity of GFP: intensive, moderate, and weak. We observed 1,392 embryos from 10 pairwise crosses of heterozygotes and found that intensive, moderate, and weak GFP groups accounted for 25%, 48%, and 27%, respectively, suggesting that GFP segregation accorded with Mendel's law of segregation.

To elucidate the function of the trapped gene during zebrafish development, the morphological defects of this mutant line were analyzed. Homozygous *add1*$^{-/-}$ mutant embryos with intensive GFP expression normally developed until 20 hpf, showing dark heads. At 24 hpf, significant abnormalities could be observed in *add1*$^{-/-}$ mutants compared with siblings, including abnormal midbrain-hindbrain boundary (MHB) (Figure 1B), smaller heads, smaller eyes, and a defective yolk extension. As development proceeds, additional morphological changes can be observed, such as swelling of the fourth ventricles and heart edema at 48

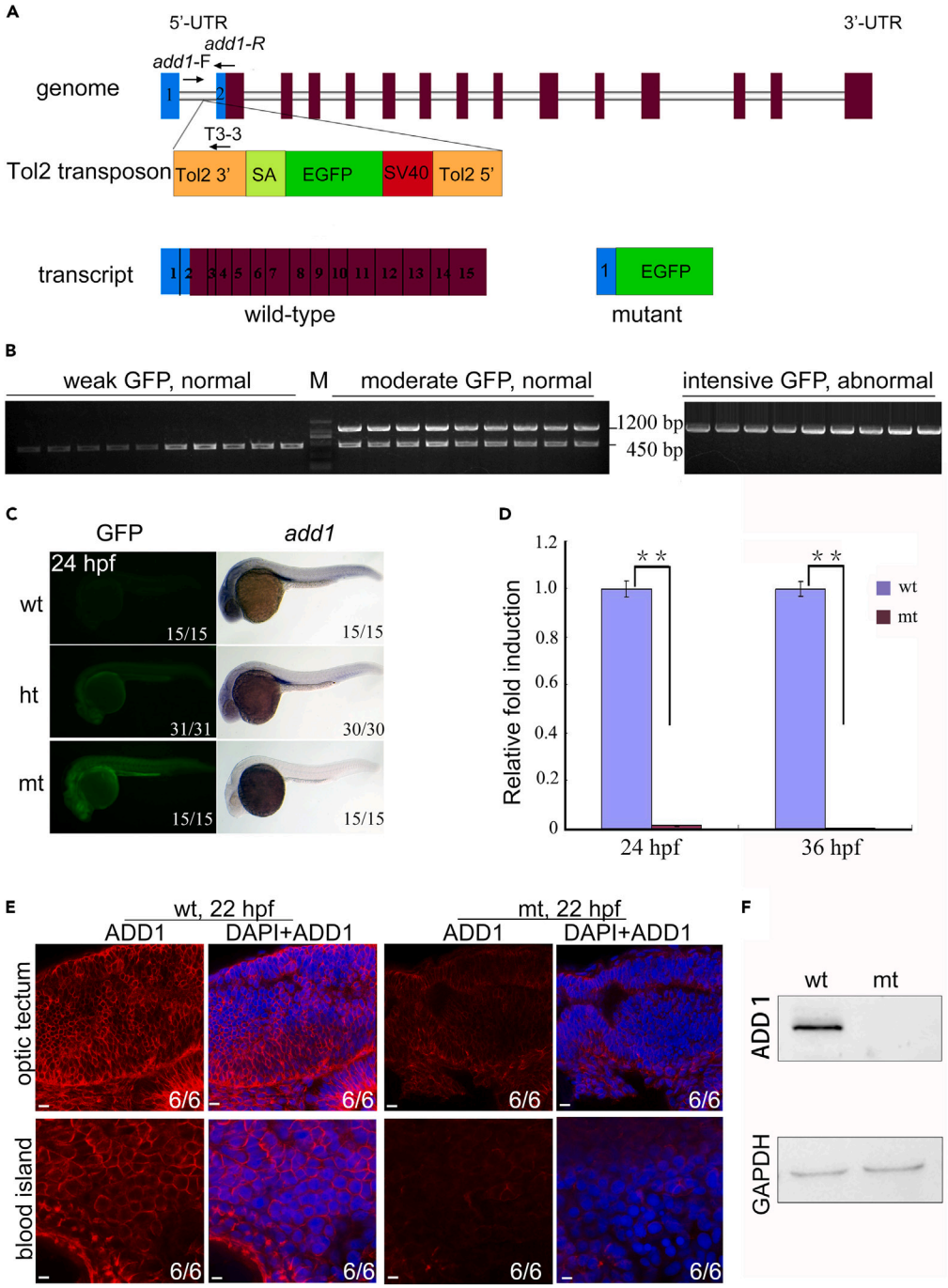

Figure 2. Genomic schematic and reduced expression level of *add1* in *add1*$^{-/-}$ mutant embryos

(A) Genomic structure of the *add1* locus and putative transcripts. The Tol2 transposon was inserted into the first intron of the *add1* gene. The binding positions and directions of primers *add1*-F, *add1*-R, and T3-3 used in (B) were indicated. UTR, untranslated region.

(B) PCR-based genotyping of individual embryos. At 24 hpf, embryos from *add1* heterozygote intercrosses were separated based on GFP intensity and phenotypes. Three primers, *add1*-F, *add1*-R, and T3-3, the Tol2-3′ element located downstream of the insertion site, were used in tandem for PCR with genomic DNA from a single embryo as the template. The mutant and WT *add1* alleles were represented by 1200 and 450 bp bands, respectively. M stands for molecular marker lane.

(C) Expression levels of *add1* transcript in mutant embryos detected with WISH. In the left panel, wt, ht, and mt represented WT with weak GFP, heterozygote with moderate GFP, and homozygote with intensive GFP, respectively. It is worth noting that the expression level of Add1 nearly vanished.

Figure 2. *Continued*

(D) qRT-PCR analysis of the relative expression level of *add1* in WT and *add1*$^{-/-}$ embryos at indicated stages. *β-actin* was used as an internal control. Embryos were pre-sorted as mentioned above. The data were presented as mean ± SD from three independent biological repeats. Total RNA of each group was extracted from a pool of 30 embryos. **, $p < 0.01$ (by Student's *t* test).

(E and F) Expression of Add1 was dramatically reduced in *add1*$^{-/-}$ mutants. Embryos of *add1*$^{-/-}$ and their siblings were harvested at 22 hpf, and then stained with anti-Add1 antibodies. Confocal photography was used to capture the optic tectum and blood island. (E). Scale bars, 10 μm. The levels of Add1 in cell lysis of the embryos was further analyzed by western blots (F).

hpf (Figure 1B). In addition to dysplasia, the number of blood cells in circulation significantly decreased in mutant animals. At 30 hpf, zebrafish already have blood circulation, and some blood cells can be seen in the caudal veins of wild type (WT) embryos. In contrast, there are almost no blood cells in mutant embryos can be seen (Figure 1C). Over time, the severity of the defects increased and the mutants died around 5 dpf. Taken together, we obtained a zebrafish mutant with significant abnormalities in development.

The interruption of the *add1* locus accounts for the mutant phenotype

To identify the Tol2 integration site in the mutant line, we performed 5′-rapid amplification of cDNA ends (5′-RACE) on total RNAs isolated from homozygous embryos at 24 hpf. The sequencing result of the 5′-RACE products showed that the first exon of the zebrafish *add1* gene was fused with GFP (Figure S1A). This finding confirmed that the gene disrupted by the Tol2 transposon in the mutant embryos is *add1*. Zebrafish *add1* is located on chromosome 21 and encodes a 783 amino acid protein with 76% identity to human *ADD1* (Figure S1B).

The *add1* locus in zebrafish comprises 13 exons and 12 introns. The transposon element insertion occurs at the first intron, allowing the transcription of the GFP expression cassette under the control of the *add1* promoter (Figure 2A). Using PCR-based genotyping, specific primers *add1*-F, *add1*-R, and T3-3 were designed to test the relationship between GFP expression levels and the interrupted *add1* locus. The results show that intensive GFP-embryos and moderate GFP-embryos in this mutant line had homozygous and heterozygous insertions of the Tol2 transposon at the *add1* locus, respectively. At the same time, embryos with weak GFP do not have Tol2 elements inserted (Figure 2B). This suggested that GFP expression was closely related to the mutant line's phenotypes.

Subsequently, we utilized several approaches to verify that the mutation in *add1* mutants is sufficient to cause the phenotype. We first used whole-mount RNA *in situ* hybridization (WISH) to look at the expression of *add1* in this mutant. The WISH results revealed that *add1* was expressed both maternally and zygotically throughout early development (Figure S2A), with relative enrichment in the head and anterior region of the pronephric ducts at 22 hpf (Figure S2A). By 36 hpf, add1 transcripts were also found in hematopoietic tissue (Figure S2A). At 24 hpf, we found that *add1* expression was robust in WT siblings but significantly reduced or abolished in homozygotes (Figure 2C).

We accessed the relative abundance of endogenous *add1* transcript in WT and mutant embryos by quantitative real-time PCR (qRT-PCR). The results indicated that homozygous embryos at 24 hpf and 36 hpf only retained approximately 0.014% and 0.004% amount of *add1* mRNA in the WT embryos, respectively (Figure 2D).

We next performed immunofluorescence analysis with an anti-Add1 antibody to visualize Add1 distribution in the mutant embryos. In WT embryos, the expression of Add1 is robust and mainly localized at the membrane in all examined cells, while in the mutant embryos, a profound reduction of Add1 was observed when detected with immunostaining (Figure 2E). At the same time, the protein level of Add1 was reduced profoundly in the mutant when analyzed with western blot (WB) (Figure 2F).

We also used Morpholino injection to knock down *add1* in zebrafish embryos. Injection with 10 ng of *add1*-MO efficiently blocked *add1*-5′UTR-EGFP reporter expression (Figures S3A and S3B). The morphants injected with 10 ng or 15 ng of *add1*-MO exhibited phenotypic traits consistent with those observed in *add1*$^{-/-}$ mutants at 30 hpf and 48 hpf, including a curved body axis, reduced circulating blood cells, hydrocephalus, and edema (Figures S3C and S3D). Furthermore, *o*-dianisidine staining of the morphants at 30 hpf and 48 hpf revealed significantly diminished or absent signals compared to WT embryos

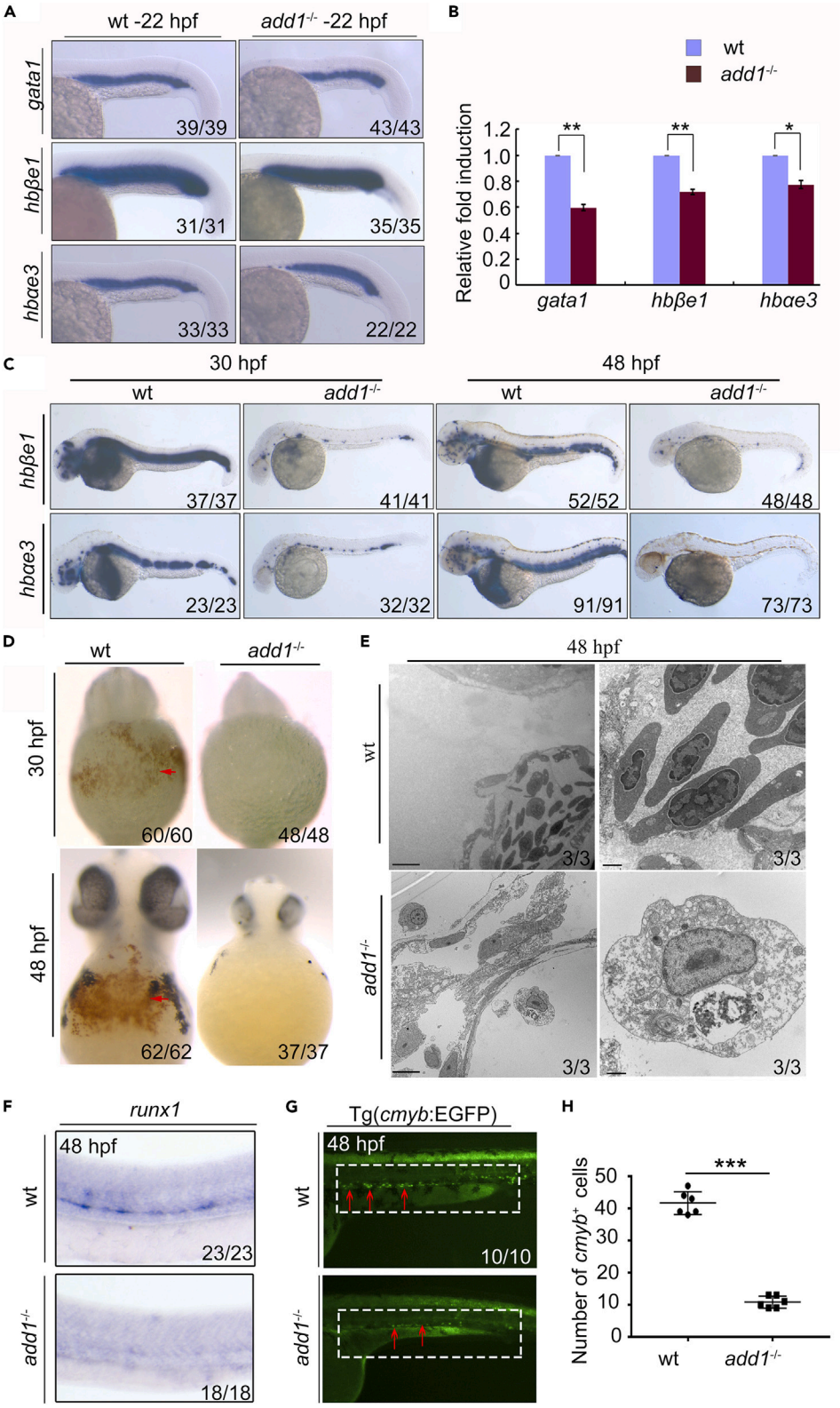
A
wt -22 hpf
add1-/- -22 hpf
gata1
hbβe1
hbαe3
39/39
43/43
31/31
35/35
33/33
22/22
B
wt
add1-/-
Relative fold induction
1.2
1.0
0.8
0.6
0.4
0.2
0
**
**
*
gata1
hbβe1
hbαe3
C
30 hpf
48 hpf
wt
add1-/-
wt
add1-/-
hbβe1
hbαe3
37/37
41/41
52/52
48/48
23/23
32/32
91/91
73/73
D
wt
add1-/-
30 hpf
48 hpf
60/60
48/48
62/62
37/37
E
48 hpf
wt
add1-/-
3/3
3/3
3/3
3/3
F
runx1
48 hpf
wt
add1-/-
23/23
18/18
G
Tg(cmyb:EGFP)
48 hpf
wt
add1-/-
10/10
H
***
Number of cmyb+ cells
50
40
30
20
10
0
wt
add1-/-

Figure 3. *add1* is required for the primitive erythropoiesis and definitive hematopoiesis

(A) Expression pattern of primitive erythropoiesis marker genes in *add1* mutant embryos. The erythrocyte marker genes *gata1*, *hbαe3* and *hbβe1* were detected with WISH in *add1* mutant and siblings at 22 hpf. There was a slight decrease in the expression levels of these genes in the mutants.

(B) FPKM values of erythroid cell specific genes in $add1^{-/-}$ and siblings.

(C) WISH results of erythrocyte marker genes from 36 hpf to 48 hpf. The expression levels of *hbαe1* and *hbβe3* in *add1* mutant embryos decreased sharply in the mutant from 30 hpf to 48 hpf.

(D) *o*-dianisidine staining for hemoglobin at indicated embryos. Left panel: Hemoglobin in red blood cells is strongly stained in WT embryos, noted prominently in the ducts of cuvier over the yolk sac (red arrow). Right panel: In contrast, there is no detectable hemoglobin staining in *add1* mutant embryos.

(E) Transmission electron micrographs of WT and $add1^{-/-}$ erythrocytes at 48 hpf. Note that erythroid cells from $add1^{-/-}$ heart chambers were variable in the number and morphology, the bottom looked like erythroblast. Scale bars: 5 μm (left panel); 500 nm (right panel).

(F) Expression pattern of *runx1* in $add1^{-/-}$ mutants and WT siblings. The expression level of *runx1* decreased in mutant embryos at 48 hpf.

(G) The EGFP signals in the mutant embryos in the background of Tg(*c-myb*:EGFP). The EGFP positive signals displayed an obvious reduction of HSCs compared with WT embryos at 48hpf. The red arrows indicate *c-myb* expression.

(H) Quantification of $c\text{-}myb^{+}$ HSPCs. Error bars, mean ± SD, ***, $p < 0.001$.

(Figures S3E and S3F). To assess rescue potential, mRNA rescue experiments were conducted in $add1^{-/-}$ embryos. Introduction of 100 or 200 pg of *add1* mRNA, synthesized *in vitro*, into *add1* mutant embryos at the one-cell stage partially reversed the anemic abnormalities at 30 hpf (Figures S3G and S3H). Taken together, these results confirmed that *add1* is the mutated gene responsible for the $add1^{-/-}$ mutant phenotype.

Disruption of *add1* leads to hematopoietic defects in zebrafish larva

To investigate the defects in *add1* mutant embryos, we first examined the embryos under a dissection microscope from 30 hpf to 96 hpf. We noticed that $add1^{-/-}$ larvae always had fewer blood cells compared to siblings. Blood cells were actively circulating in WT embryos at 30 hpf (Video S1, Figure 1C), but *add1* mutant embryos had only about 30 cells in circulation on average (Video S2, Figure 1C). At 96 hpf, WT embryos have 1000–3000 blood cells in circulation, whereas *add1* mutant embryos have no blood cells. This evidence suggests that *add1* plays an important role in zebrafish hematopoiesis.

To rule out the possibility that the hematopoietic defects observed in the add1 mutant were secondary effects of a vascular deficiency, we analyzed the expression of vascular marker genes, *flk* and *fli1*, by WISH. The results show that there were no obvious defects in vascular morphogenesis in *add1* mutant embryos at the indicated stages (Figure S4), indicating that the hematopoietic phenotype is not a side effect of a vascular defect.

add1 is required for primitive erythropoiesis and definitive hematopoiesis

All vertebrates, including zebrafish, have two waves of hematopoiesis.[26] To investigate the effects of *add1* deficiency on primitive erythropoiesis in $add1^{-/-}$ mutant embryos, we performed WISH for several erythroid-specific marker genes at different stages. *Gata1* was one of the first markers for erythroid lineage specification.[27] The results demonstrated that the expression levels of *gata1* were slightly lower in the mutant embryos compared to their siblings at 22 hpf (Figures 3A and S5A). Similarly, the expression levels of *hbαe3* and *hbβe1*, which are marker genes for erythrocytes, were somewhat reduced in $add1^{-/-}$ mutant embryos at 22 hpf when compared to their sibling counterparts (Figures 3A and S5A). Furthermore, by using qRT-PCR, *gata1*, *hbβe1* and *hbαe3* relative expression levels in $add1^{-/-}$ mutants were quantified. The analysis demonstrated that at 22 hpf, *add1* mutants had lower expression levels of *gata1*, *hbβe1* and *hbαe3* than WT siblings (Figure 3B). These findings indicate that $add1^{-/-}$ embryos exhibit altered initiation of erythropoiesis. When the embryos developed into 30 and 48 hpf, the expressions of *hbαe3* and *hbβe1* were significantly reduced in $add1^{-/-}$ homozygotes (Figure 3C).

To further analyze the defects in erythropoiesis, *o*-dianisidine staining was performed, which detects heme present in hemoglobin. After circulation begins, the *o*-dianisidine positive cells mainly aggregate prominently in the ducts of cuvier at 30 hpf and 48 hpf (Figure 3D). In contrast, all the $add1^{-/-}$ homozygotes had no detectable signals from 30 hpf to 48 hpf (Figure 3D), suggesting a defect in the production or maintenance of mature erythroid cells in the mutant embryos.

Following that, we wanted to observe the morphology of the remaining rare blood cells in *add1*$^{-/-}$ mutant larvae. Transmission electron microscopy (TEM) was used to examine the ultrastructural morphology changes in cardiac sections of embryos at 48 hpf. Not surprisingly, the total number of blood cells in mutant embryos at 48 hpf was greatly reduced (Figure 3E). The remaining blood cells in *add1*$^{-/-}$ embryos showed earlier proerythroblast morphology with large round cells and large non-condensed nuclei (Figure 3E), whereas the differentiated and mature red cells in WT sibling embryos were nucleated with condensed nuclei and elliptical (Figure 3E). This suggested that erythrocyte maturation was halted in *add1* deficient embryos. Overall, these findings indicate that Add1 play a vital role in promoting erythroid maturation.

We also detected the expression of the hematopoietic genes *runx1* and *c-myb*, which are thought to be markers of definitive hematopoietic stem cells (HSC) in zebrafish. The expression of *runx1* was reduced in mutant embryos detected with WISH at 48 hpf (Figure 3F). At 48 hpf, the *add1*$^{-/-}$ embryos in the background of Tg (*c-myb*: EGFP) transgenic line also showed a reduced number of EGFP-positive cells compared to WT siblings (Figures 3G and 3H), indicating that HSC formation was disrupted. Taken together, Add1 plays pivotal roles in primitive erythropoiesis and definitive hematopoiesis.

Erythrocyte membrane cytoskeleton changed in *add1* mutant embryos

Evidence suggested that Add1 played roles in membrane skeleton assembly and/or stabilization of the spectrin-actin complex in red blood cells (RBCs).[1] We speculated that a deficiency of *add1* may destroy the structure of the erythroblast. To test this, we used phalloidin-TRITC staining to examine the distribution of actin oligomers in the erythrocyte cytoskeleton of *add1* mutant embryos in the background of Tg (*gata1*:EGFP) which is widely used for monitoring living erythroid precursors. Actin filaments are abundant in WT erythroblast cells and form a highly cross-linked network (Figure 4A) while erythrocytes in mutant embryos have almost no actin filaments (Figure 4A). This data indicates that Add1 plays a role in the formation of the erythrocyte actin network, consistent with the findings in other cells.[1,28]

TEM was used to further investigate the ultrastructural membrane changes in *add1* deficient erythroblasts. TEM analysis of erythroblasts revealed that WT cells have sharply packed and organized membranes with high electron density, whereas mutant erythroblasts have membrane integrity loss and diffused membranes with low electron density (Figure 4B).

Erythrocytes' spectrin-based membrane skeleton is well known for providing blood cells with the strength and flexibility needed to deal with hemodynamic challenges in the vascular system.[29] The abnormal actin meshwork, we hypothesize, made the erythrocyte too fragile to withstand pressure from the circulation and vascular vessels. To test the hypothesis, a T2EGEZ8 mutant with no heartbeat and circulation but normal hematopoiesis[30] was crossed into *add1*$^{-/-}$ mutant. When WT embryos were stained with *o*-dianisidine at 24 hpf, 28 hpf, and 32 hpf, *o*-dianisidine positive signals were found in the intermediate cell mass (ICM) region (Figure 4C), where erythroid precursors further develop and enter the circulation by 24–26 hpf.[30] We were surprised to discover that embryos of *add1*$^{-/-}$; *tpm4*$^{-/-}$ double mutant have the same severe congenital anemia defects (Figure 4C). These results suggested that the erythrocyte membrane and its cytoskeleton changed in *add1* mutant embryos but a lack of heartbeat could not reverse the anemia phenotype.

Depletion of *add1* upregulates the p53 signal and knockout of *p53* can partially rescue the anemia phenotype

Based on the fact that Add1 interacts with RNA polymerase II and transcriptional factors in the nucleus,[15,16] we hypothesized that Add1 may regulate the transcriptional levels of target genes involved in zebrafish erythropoiesis. To better understand the nuclear-specific function of Add1, we used RNA sequencing (RNA-seq) to analyze transcriptome changes in *gata1*-EGFP positive cells sorted from *add1*-deficient embryos and siblings at 22 hpf, when the differences in the number of erythrocytes were not yet evident in *add1* mutant embryos. Among the detectable mRNAs, there were 507 differentially expressed mRNAs in total, including 412 with upregulated expression and 95 with downregulated expression (fold-change > 2, and $p < 0.05$) (Figure 5A, GSE236659). Functional annotation of differentially expressed mRNAs was performed using Gene Ontology (GO) and KEGG pathway analysis.

Based on GO annotation, the downregulated genes were enriched in the GO terms of gas transport, oxygen transport, DNA replication initiation, erythrocyte differentiation, erythrocyte homeostasis, and

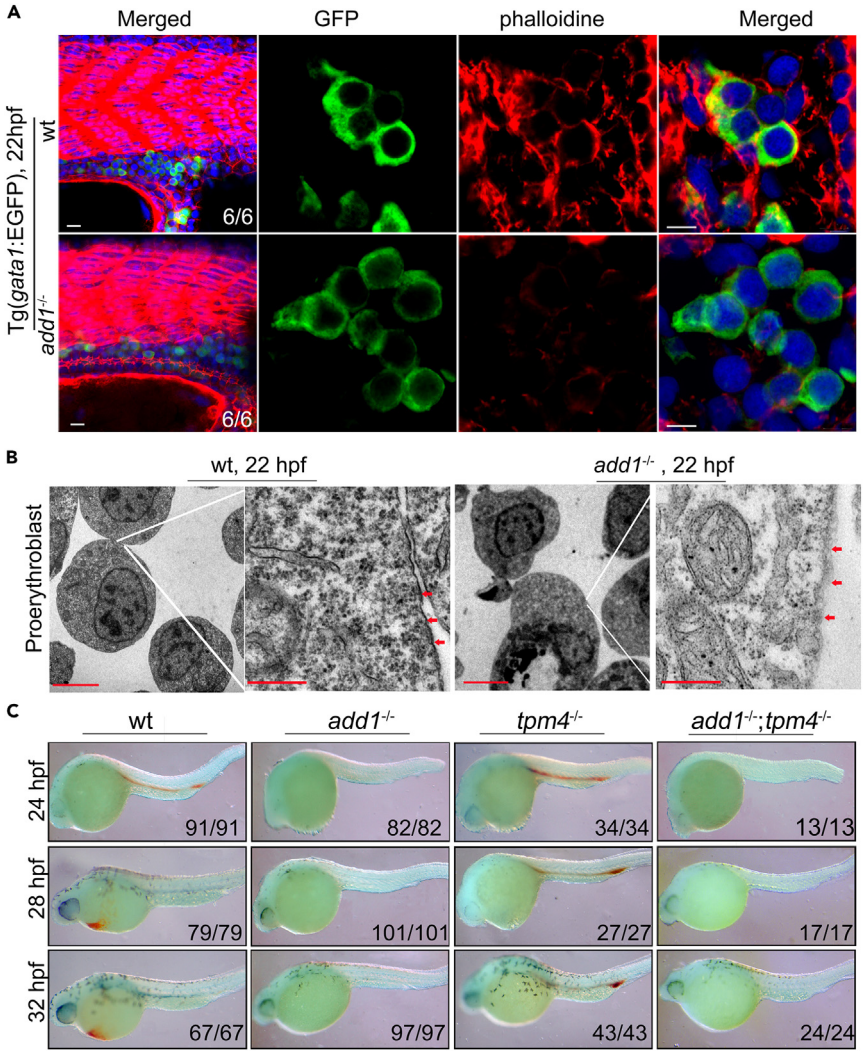

Figure 4. Abnormal cytoskeleton and ultrastructural analysis of the membrane of erythroblasts in *add1* mutant embryos

(A) Distribution of F-actin in erythroblasts. In order to display the distribution of F-actin (red) in erythroblasts, WT and mutant embryos were co-stained with phalloidin-TRITC and anti-GFP antibody at 22 hpf (green). Confocal fluorescence microscopy was used to examine the sagittal cryosections. Scale bars: 10 μm (left panel); 5 μm (right panel).

(B) TEM ultrastructural examination of the proerythroblast membrane in the *add1* mutant. On the right panel, labeled regions on the left panel were enlarged. The images are representative of 4 embryos each. Scale bars: 10 μm (left panel); 500 nm (right panel).

(C) *o*-dianisidine staining of *add1* mutant and double mutant of *add1*;*tpm4* at indicated stages. Embryos were sorted to four groups by the phenotype of mutant *add1* and *T2EGEZ8*. Embryos had no heart beat and shrinkage of yolk sac extension; smaller head and a few pigments were double mutant carried *add1* and *tpm4* gene. Note that there are no detectable positive signals in the double mutants just like the mutant of *Add1*. In *T2EGEZ8* mutant, the positive signals were only found in the ICM from 24 hpf to 32 hpf.

myeloid cell homeostasis (Figure S6A). The upregulated genes were mainly enriched in supramolecular fiber organization, actin filament-based process (Figure S6A). According to the KEGG pathway analysis, p53, apoptosis, and cell cycle signaling pathways were significantly upregulated in the *add1*-deficient erythrocytes (Figure 5B). Among significantly enriched pathways, the activated p53 signaling pathway interested us (Figures 5A and S6B). Expression levels of *p53* and its target genes, such as *mdm2*, *casp8*, and *gaddaa* were confirmed to be elevated in *add1*-deficient embryos by qRT-PCR (Figure 5C) and WISH (Figure 5D).

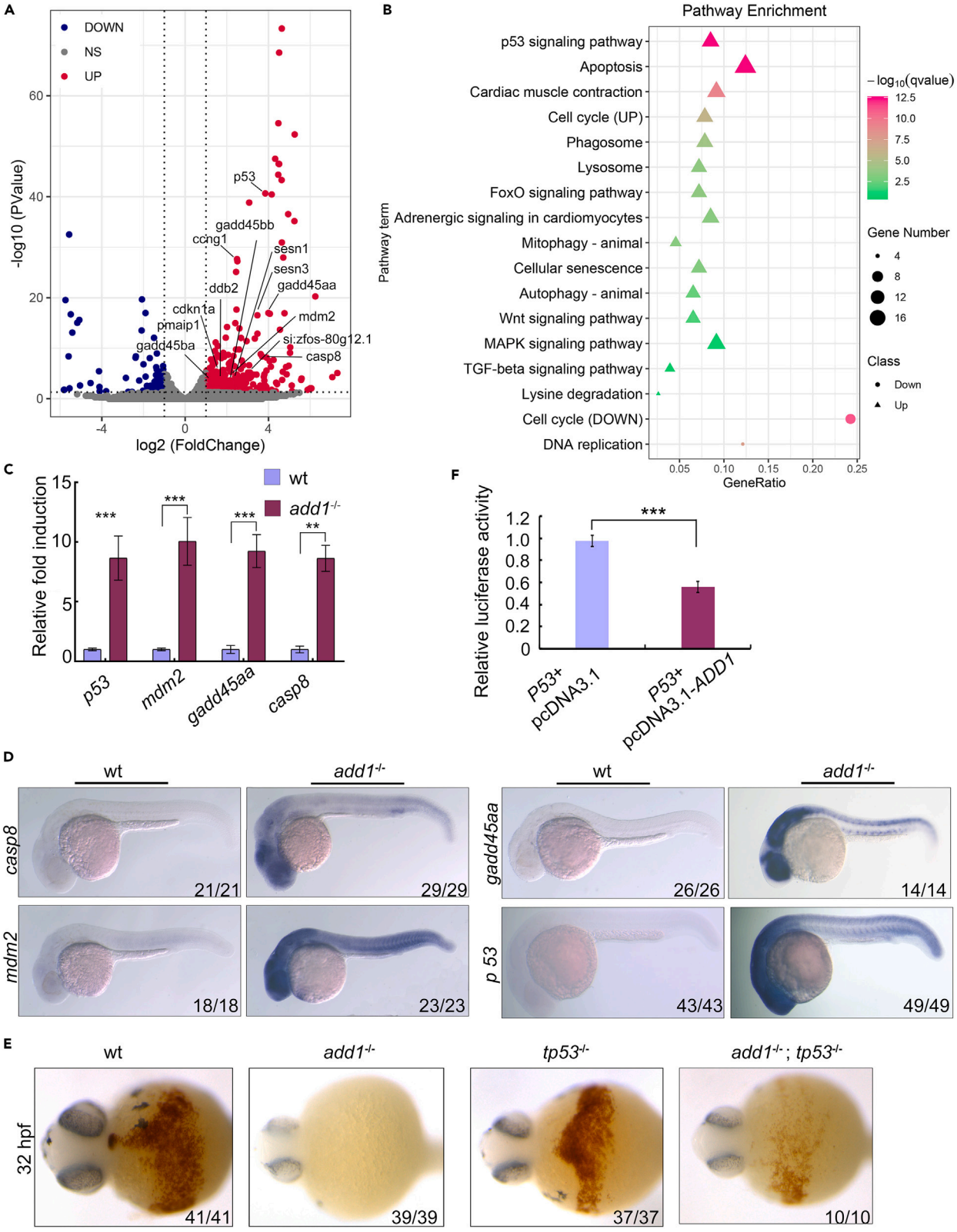
A
DOWN
NS
UP
-log10 (PValue)
log2 (FoldChange)
p53
gadd45bb
ccng1
sesn1
sesn3
gadd45aa
ddb2
cdkn1a
pmaip1
mdm2
si:zfos-80g12.1
gadd45ba
casp8
B
Pathway Enrichment
p53 signaling pathway
Apoptosis
Cardiac muscle contraction
Cell cycle (UP)
Phagosome
Lysosome
FoxO signaling pathway
Adrenergic signaling in cardiomyocytes
Mitophagy - animal
Cellular senescence
Autophagy - animal
Wnt signaling pathway
MAPK signaling pathway
TGF-beta signaling pathway
Lysine degradation
Cell cycle (DOWN)
DNA replication
Pathway term
GeneRatio
−log10(qvalue)
Gene Number
Class
Down
Up
C
wt
add1-/-
Relative fold induction
p53
mdm2
gadd45aa
casp8
F
Relative luciferase activity
P53+ pcDNA3.1
P53+ pcDNA3.1-ADD1
D
wt
add1-/-
casp8
21/21
29/29
gadd45aa
26/26
14/14
mdm2
18/18
23/23
p 53
43/43
49/49
E
wt
add1-/-
tp53-/-
add1-/- ; tp53-/-
32 hpf
41/41
39/39
37/37
10/10

Figure 5. Elevated *p53* is responsible for the survival of the erythroblast

(A) Volcano plot of differentially expressed coding genes (DEGs) between erythroblast from *add1*$^{-/-}$ and siblings. Vertical lines correspond to 2-fold differences; horizontal line represents a p value of 0.05. Red and blue points represent DEGs with statistical significance. The differentially expressed genes enriched in p53 signaling pathway were indicated.

(B) Pathway enrichment analysis identified affected in mutants.

(C) The expression levels of *p53* related genes were examined by qRT-PCR. The expression levels of *β-actin* were used as a reference to normalize the amounts of mRNAs in each group. Significance of differences: **, $p < 0.01$, ***, $p < 0.001$ (by Student's *t* test).

(D) Expression pattern of *p53* related genes in *add1* mutant embryos detected by WISH. The expression levels of these genes were elevated in *add1* mutant embryos.

(E) Detection of hemoglobin in different embryos using *o*-dianicidine staining. Note that there are apparent positive signals in the *add1*;*p53* double mutants embryos at the indicated stage.

(F) Dural luciferase reporter assay of ADD1 regulating the *p53* promoter. Confirmation of Add1 inhibiting the promoter activity of *p53*. ***, $p < 0.001$ (by Student's *t* test).

We wanted to know if removing *p53* from the embryos can rescue the anemic phenotype. As a result, *add1* heterozygous adults were crossed with *p53* homozygous mutant adults, yielding double mutant embryos. The hemoglobin level was also determined using *o*-dianisidine staining. We found that the expression of hemoglobin was improved at 32 hpf in *add1*;*p53* double mutant embryos compared *to add1* mutant embryos (Figure 5E). We then performed a dual-luciferase reporter gene assay to test the effect of Add1 on *p53* promoter activity, Figure 5F showed that ADD1 decreased the *p53* promoter activity to about 50% of control. Taken together, these findings suggest that the anemic phenotype due to *add1* deletion is partially dependent on the p53 signaling pathway.

add1 deficiency causes apoptosis

It is well known that *p53* is a famous activator of apoptosis, which inspires us to detect apoptosis in *add1* mutant embryos. TUNEL assay revealed that apoptosis signals were much higher in the brain, spinal cord, and ICM region in *add1*$^{-/-}$ mutants than in the WT siblings (Figures 6A and 6C) at 28 hpf. We attempted to know whether the reduction of erythrocytes was due to apoptosis and performed a TUNEL assay on *add1* mutant embryos in the background of Tg (*gata1*:EGFP) zebrafish. We found that apoptosis signals were enriched in *gata1*-EGFP positive cells at the 14-somite stage and 22 hpf (Figures 6B and 6C), suggesting erythroblast cells maybe undergo apoptosis. We sought to investigate whether the deficiency of *add1* resulted in the phenotype of erythroid cells by activating the p53-mediated apoptotic pathway. To address this, we microinjected *p53* MOs and performed a TUNEL assay to assess erythrocyte apoptosis in *add1*$^{-/-}$ embryos at 22 hpf. The results demonstrated a significant reduction in apoptotic signals within *gata1*$^{+}$ cells of *add1*$^{-/-}$ embryos following *p53* knockdown, as compared to WT embryos (Figures 6C and 6D).

Meanwhile, TEM revealed that many mutant proerythroblasts had more mitochondria, nuclear budding, fragmentation, and vacuolated cytoplasm, which are all ultrastructural characteristics of apoptosis (Figure 6E). Thus, these findings indicate that the loss of *add1* caused apoptosis in erythroid progenitors in *add1* mutant embryos.

DISCUSSION

In this study, we obtained a zebrafish mutant *add1*$^{-/-}$ using Tol2 transposon-mediated gene trapping methods, in which the interrupted gene was zebrafish *add1*. Embryos homozygous (mutant) for the transposon insertion are characterized by lack of blood cells in circulation, heart edema, smaller head, and eyes, striking dilation of the fourth ventricles, reduced melanocytes, and shrinkage of yolk sac extension and die at 5 dpf. In *add1* homozygous mutant embryos, primitive erythropoiesis, and definitive hematopoiesis were affected. Mutant embryos suffered from extensive apoptosis in the brain, spinal cord, and ICM region, and erythroblast cells underwent apoptosis as early as 14-somites stage. The ultrastructural membrane of proerythroblasts in the add1 mutant showed compromised integrity and exhibited membrane diffusion. Our findings provide evidence for the first time that accelerated apoptosis and defective assembly of membrane proteins in erythroid precursors are due to *add1* deficiency in our zebrafish anemia model.

Although hemolytic anemia caused by targeted deletion of *add1* has been reported in mammals,[3] this is the first report in a non-mammalian vertebrate animal model in our study. Unlike the zebrafish *add1* mutant, which is embryonic fatal at around 5 dpf, these mice are alive and reach maturity. To date, there is no report on pathological consequences of *ADD1* defects with mild to severe anemia in humans. Mouse red cells deficient in *add1* are characterized by spherocytes with significant loss of surface area, decreased mean corpuscular

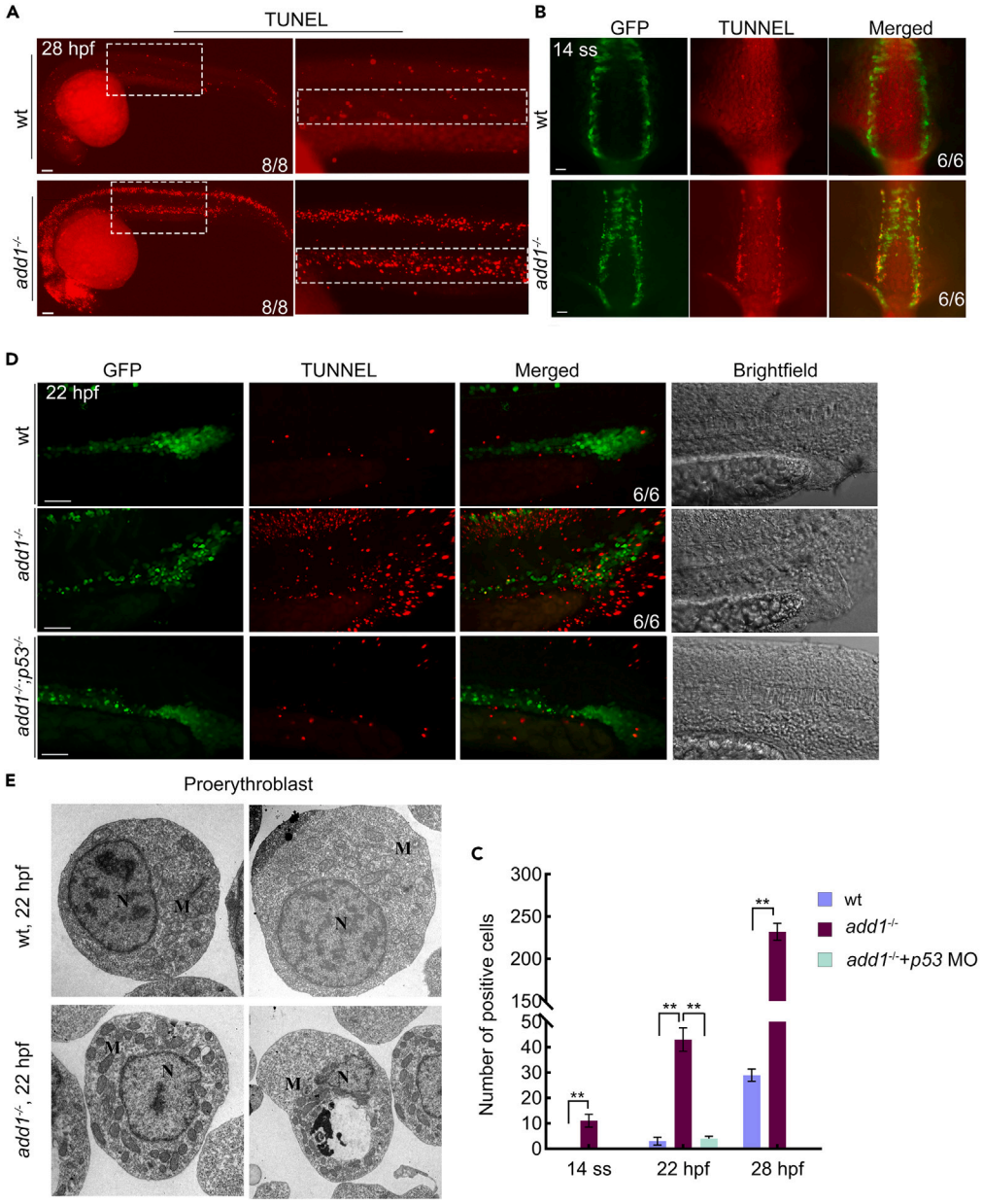

Figure 6. Excess apoptosis occurred in *add1* mutant embryos

(A) DNA fragmentation was detected by TUNEL assay. Embryos were observed by fluorescence microscopy after staining at indicated stages. Note that the mutants had more and stronger positive signals. Scale bars: 100 μm.

(B) TUNEL assay in embryos under the background of Tg (*gata1*:EGFP) at 14-somites stage. Scale bars: 100 μm.

(C) Statistical data for the number of TUNEL positive cells. The positive cells are defined by ImageJ software in 6 WT and mutant siblings. Significance of differences:**, $p < 0.01$ (by Student's *t* test).

(D) TUNEL assay in embryos under the background of Tg (*gata1*:EGFP). The embryos of WT, *add1*$^{-/-}$ and *add1*$^{-/-}$ microinjected with *p53* MO were harvested at 22 phf and conducted with TUNEL assay. The images were taken by confocal fluorescence microscopy. Scale bars: 50 μm.

(E) Ultrastructure of proerythroblast in mutant embryos observed by TEM. Blood island region of WT and mutant homozygous embryos were sectioned and observed by TEM. Note that the increased number of mitochondria (indicated by arrowhead) can be seen in proerythroblast of mutant siblings in contrast with WT siblings. N, nuclear; M, mitochondria.

volume (MCV), cell dehydration, and increased osmotic fragility.[3] This supported that Add1 plays an important role in maintaining RBC membrane stability. However, the mechanism of hemolytic anemia occurrence is not clear. As zebrafish is a powerful vertebrate model for the study of hematopoiesis and other aspects of embryogenesis and organogenesis.[31] Analysis of the mutant *add1* homozygous embryos will provide important clues for the mechanism of blood anemia and developmental roles in hematopoiesis.

All vertebrates have two waves of hematopoiesis, primitive and definitive hematopoiesis.[26] In zebrafish, primitive hematopoiesis occurs in two locations: the intermediate cell mass and the rostral blood island. Cells within the ICM differentiate into the endothelial cells of the trunk vasculature and proerythroblasts, which begin to enter the circulation at 24 hpf.[31] We employed WISH to investigate the early erythropoiesis of *add1*$^{-/-}$ mutant embryos. At 22 h postfertilization (hpf), these homozygous mutants exhibited modestly reduced expression levels of key erythroid cell-related genes, including *gata1*, *hbαe3*, and *hbβe1* (Figure 3A). This observation implies a compromised initiation of primitive erythropoiesis in these mutant embryos. *o*-dianisidine staining for hemoglobin was performed to check whether red cell maturation is normal. The results indicated that the mature blood cells were almost absent in *add1* mutant and *add1* morphant embryos (Figures 3D and S3E). Meanwhile, mature hematopoietic cell markers, such as *hbαe3* and *hbβe1* were all found to be significantly down-regulated from 30 to 48 hpf detected by WISH (Figure 3C). Between 36 and 48 hpf, primitive circulating erythroblasts have a rounded shape and develop into erythrocytes with a lentiform appearance.[32] But the remaining blood cells in circulation displayed morphological abnormalities, including an apparent maturation arrest at the proerythroblast stage (Figure 3E). Therefore, disrupting *add1* resulted in not only fewer erythrocytes but also the repression of proerythroblast maturation. Further studies may provide insights into the role of Add1 in erythrocyte maturation in zebrafish.

However, the expression levels of *runx1* and *c-myb*, known as definitive hematopoiesis marker genes, decreased dramatically (Figures 3F–3H). This supports that the process of definitive hematopoiesis is affected in the *add1*$^{-/-}$ mutant embryos. These data demonstrated that *add1* is involved in primitive erythropoiesis and definitive hematopoiesis.

It has been demonstrated that many actin-binding proteins and actin-related proteins are involved in nuclear-specific functions such as chromatin remodeling, transcription, and nuclear transport.[33] ADD1, a NLS-containing actin-binding protein, can shuttle between the cytoplasm and nucleus. ADD1 translocates into the nucleus upon loss of cell-cell adhesion.[15] ADD1 binds to and co-localizes with RFX-1 in the nucleus, implying a role in some nuclear-specific functions.[17] In the nucleus, ADD1 interacts with RNA polymerase II and the transcriptional factor ZNF331, but the mechanism by which ADD1 regulates transcription remains unknown.[16] In our investigation, we employed RNA-seq to conduct a comprehensive screening of potential transcriptional targets influenced by Add1. Our findings unveiled the activation of multiple genes associated with the p53 pathway in *add1*-deficient embryos (Figures 5A and 5B). Subsequent validation through qRT-PCR and WISH assays confirmed the upregulation of *p53* and its target genes in *add1*-deficient embryos (Figures 5C and 5D). Furthermore, our reporter gene assay (Figure 5F) demonstrated a significant reduction in promoter activity of *p53* upon the modulation of *ADD1*, implying that *ADD1* could regulate *p53* at the transcriptional level.

Additionally, we used the TUNEL assay to show that p53-mediated apoptosis was induced in *add1*-deficient embryos (Figures 6A and 6C), the apoptosis occurred in proerythroblast cells early at the 14-somites stage (Figure 6B). Given that the TUNEL assay is capable of detecting signals during the initial stages of apoptosis when cell disintegration has not yet occurred, it is expected that there would be no notable differences in cell numbers. Consequently, the expression level of *gata1* did not exhibit a significant decrease at 24 hpf (Figure 6D). Interestingly, when compared to *add1* homozygous mutant embryos, the *o*-dianisidine staining defects in *add1*;*p53* double mutant embryos were partially rescued. The data demonstrated that apoptosis in proerythroblasts is partially *p53* dependent. The residual blood cells observed in *add1* homozygous mutant embryos exhibited proerythroblast morphology characterized by enlarged round cells and non-condensed nuclei, as evidenced in Figure 3E, indicating impaired erythrocyte development. Our RNA-seq analysis of *gata1*$^{+}$ cell sorting from *add1*$^{-/-}$ embryos or siblings revealed an enrichment of differentially expressed genes, particularly within the cell cycle and other pathways (Figures 5A and 5B). Notably, the upregulation of cell cycle-related genes *p53*, *mdm2*, and *gadd45aa* was observed, suggesting a potential arrest in the cell cycle. Previous studies have demonstrated that cell cycle inhibition or exit can lead to abnormal cell differentiation,[34] which in some circumstances may

result in apoptosis.[35] Furthermore, *p53* has been identified as a crucial regulator of cell-cycle arrest and initiation of apoptosis.[36] Thus, we propose a hypothesis that the elevated expression of genes associated with the p53 pathway may contribute to the induction of apoptosis in proerythrocytes of *add1*-deficient embryos by impeding the cell cycle. It will be interesting to investigate the other possible cell death mechanism involved in the mutant's elimination of proerythroblast. It has been established that Add and Band 3 work together to stabilize the cohesive forces that link the erythrocyte membrane skeleton and the bilayer. This connection can be broken by Add tail domains, resulting in membrane fragmentation on its own.[37]

Consistent with our finding, the p53 pathway is activated in some zebrafish models of hematopoietic diseases. In zebrafish, ribosomal protein S19 deficiency causes developmental abnormalities and defective erythropoiesis via the p53 pathway.[38] Higher p53 activity contributes to the phenotypes of Diamond Blackfan anemia by inducing apoptosis during RBC differentiation.[39] In telomerase-deficient zebrafish, the p53 pathway is activated.[40] During the early stages of dyskeratosis congenital pathogenesis, *dkc1,* and *nola1* deficiency in zebrafish contributes to the hematopoietic phenotype via p53 activation associated with rRNA processing defects. Loss of *p53* rescues the definitive hematopoietic phenotype in *nol9*-deficient zebrafish.[38] Our finding expands the critical roles of p53-mediated apoptosis in hematopoietic development and diseases.

Erythrocyte membrane structure is the model for all spectrin-based membrane skeletons, and abnormalities in its structure cause a variety of hemolytic anemias.[41] Add1 is a well-known protein located at the junction of actin and spectrin. It regulates the global properties of the cell, possibly including cation transport, cell morphology, and membrane deformability.[42] This enables RBCs to withstand high shear forces within the circulation and undergoes extensive deformation to squeeze through the microvasculature intact.[3] *Add1*-null mice have compensatory hemolytic anemia with hallmarks of hereditary spherocytosis RBCs, such as spherocytes with considerable surface area reduction and enhanced osmotic fragility. Add2 and Add3 are likewise missing in the RBC of Add1-null animals, demonstrating that Add1 is the limiting subunit in tetramer formation at the spectrin-actin junction.[3] We hypothesize that abnormal RBCs in the mutant with a fragile membrane skeleton cannot survive through circulation. To test this hypothesis, we crossed a mutant *tpm4*$^{-/-}$, which has no heartbeat and circulation, with an *add1* mutant. Interestingly, in the double mutant of *add1;tpm4*, the phenotype of blood anemia also happened like mutant *add1*(Figure 4C). This implies that the heartbeat and high shear forces within the circulation are not responsible for the anemia in *add1* mutant embryos.

Limitations of the study

Because *add1* is a gene expressed ubiquitously, there are also other abnormalities in the mutant such as heart edema and hydrocephalus (Figure 1B). This is supported by *Add1*-null mice. Targeted deletion of *add1* results in strain-dependent non-erythroid phenotypes such as abnormal cervicothoracic spine curvature with complete penetrance and severe megaesophagus.[43] The role of Add1 in developmental and organogenesis needs to be studied further.

STAR★METHODS

Detailed methods are provided in the online version of this paper and include the following:

- KEY RESOURCES TABLE
- RESOURCE AVAILABILITY
  - Lead contact
  - Materials availability
  - Data and code availability
- EXPERIMENTAL MODEL AND STUDY PARTICIPANT DETAILS
  - Zebrafish strains and transgenesis
  - Ethical approval
- METHOD DETAILS
  - 5′-RACE analysis
  - Genotyping and quantitative real-time PCR
  - Morpholino, mRNA, and plasmid microinjection
  - Cryosectioning and *o*-dianisidine staining
  - Whole-mount *in situ* hybridization and immunostaining
  - TUNEL assay
  - Transmission electron microscopy

- Cell sorting and RNA sequencing
- Dual-luciferase reporter gene assay
- Data analysis for gene expression

- QUANTIFICATION AND STATISTICAL ANALYSIS

SUPPLEMENTAL INFORMATION

Supplemental information can be found online at https://doi.org/10.1016/j.isci.2023.107516.

ACKNOWLEDGMENTS

This work was supported by grants from the National Natural Science Foundation of China (30900843, 82271731, 81971390). We are grateful to members of the Anming Meng and Qiang Wang Laboratory for helpful discussion and assistance.

AUTHOR CONTRIBUTIONS

S.Y. designed, performed most experiments, analyzed the data, and wrote the original draft. S.C. edited the manuscript and involved in data generation and interpretation. Q.L. analyzed the RNA-Seq results and involved in data generation. B.X., J.G., and J.L. performed *in situ* hybridization experiments, western blots and raised the zebrafish lines. S.C. and Z.J. performed dual-luciferase reporter assay. F.W. and Y.B. provided critical reagents. T.Z. discussed the results and edited the manuscript. S.S. and L.W. designed experiments, interpreted data, and revised the manuscript. All authors contributed to manuscript editing and review.

DECLARATION OF INTERESTS

The authors declare no competing interests.

Received: November 11, 2022
Revised: June 13, 2023
Accepted: July 26, 2023
Published: July 29, 2023

REFERENCES

1. Hughes, C.A., and Bennett, V. (1995). Adducin: a physical model with implications for function in assembly of spectrin-actin complexes. J. Biol. Chem. *270*, 18990–18996. https://doi.org/10.1074/jbc.270.32.18990.

2. Bennett, V., and Baines, A.J. (2001). Spectrin and ankyrin-based pathways: metazoan inventions for integrating cells into tissues. Physiol. Rev. *81*, 1353–1392. https://doi.org/10.1152/physrev.2001.81.3.1353.

3. Robledo, R.F., Ciciotte, S.L., Gwynn, B., Sahr, K.E., Gilligan, D.M., Mohandas, N., and Peters, L.L. (2008). Targeted deletion of alpha-adducin results in absent beta- and gamma-adducin, compensated hemolytic anemia, and lethal hydrocephalus in mice. Blood *112*, 4298–4307. https://doi.org/10.1182/blood-2008-05-156000.

4. Leite, S.C., Sampaio, P., Sousa, V.F., Nogueira-Rodrigues, J., Pinto-Costa, R., Peters, L.L., Brites, P., and Sousa, M.M. (2016). The Actin-Binding Protein alpha-Adducin Is Required for Maintaining Axon Diameter. Cell Rep. *15*, 490–498. https://doi.org/10.1016/j.celrep.2016.03.047.

5. Manunta, P., Burnier, M., D'Amico, M., Buzzi, L., Maillard, M., Barlassina, C., Lanella, G., Cusi, D., and Bianchi, G. (1999). Adducin polymorphism affects renal proximal tubule reabsorption in hypertension. Hypertension *33*, 694–697. https://doi.org/10.1161/01.hyp.33.2.694.

6. Beeks, E., van der Klauw, M.M., Kroon, A.A., Spiering, W., Fuss-Lejeune, M.J.M.J., and de Leeuw, P.W. (2004). Alpha-adducin Gly460Trp polymorphism and renal hemodynamics in essential hypertension. Hypertension *44*, 419–423. https://doi.org/10.1161/01.HYP.0000141410.72537.fd.

7. Lemaitre, R.N., Heckbert, S.R., Psaty, B.M., Smith, N.L., Kaplan, R.C., and Longstreth, W.T., Jr. (2002). Hormone replacement therapy and associated risk of stroke in postmenopausal women. Arch. Intern. Med. *162*, 1954–1960. https://doi.org/10.1001/archinte.162.17.1954.

8. Tobin, M.D., Braund, P.S., Burton, P.R., Thompson, J.R., Steeds, R., Channer, K., Cheng, S., Lindpaintner, K., and Samani, N.J. (2004). Genotypes and haplotypes predisposing to myocardial infarction: a multilocus case-control study. Eur. Heart J. *25*, 459–467. https://doi.org/10.1016/j.ehj.2003.11.014.

9. van Rijn, M.J.E., Bos, M.J., Yazdanpanah, M., Isaacs, A., Arias-Vásquez, A., Koudstaal, P.J., Hofman, A., Witteman, J.C., van Duijn, C.M., and Breteler, M.M.B. (2006). Alpha-adducin polymorphism, atherosclerosis, and cardiovascular and cerebrovascular risk. Stroke *37*, 2930–2934. https://doi.org/10.1161/01.STR.0000248760.67039.2b.

10. Nicod, J., Frey, B.M., Frey, F.J., and Ferrari, P. (2002). Role of the alpha-adducin genotype on renal disease progression. Kidney Int. *61*, 1270–1275. https://doi.org/10.1046/j.1523-1755.2002.00275.x.

11. Devuyst, O., Persu, A., Stoenoiu, M.S., Pirson, Y., Lens, X.M., and Chauveau, D. (2003). Enos polymorphism and renal disease progression in autosomal dominant polycystic kidney disease. Am. J. Kidney Dis. *41*, 1125. https://doi.org/10.1016/s0272-6386(03)00292-0.

12. Shen, N., Liu, C., Li, J., Chen, X., Yang, Y., Zhu, Y., Gong, Y., Gong, J., Zhong, R., Cheng, L., and Miao, X. (2015). A phosphorylation-related variant ADD1-rs4963 modifies the risk of colorectal cancer. PLoS One *10*, e0121485. https://doi.org/10.1371/journal.pone.0121485.

13. Joshi, R., and Bennett, V. (1990). Mapping the domain structure of human erythrocyte adducin. J. Biol. Chem. *265*, 13130–13136.

14. Joshi, R., Gilligan, D.M., Otto, E., McLaughlin, T., and Bennett, V. (1991). Primary structure

and domain organization of human alpha and beta adducin. J. Cell Biol. *115*, 665–675. https://doi.org/10.1083/jcb.115.3.665.

15. Chen, C.L., Lin, Y.P., Lai, Y.C., and Chen, H.C. (2011). alpha-Adducin translocates to the nucleus upon loss of cell-cell adhesions. Traffic *12*, 1327–1340. https://doi.org/10.1111/j.1600-0854.2011.01245.x.

16. Liu, C.M., Hsu, W.H., Lin, W.Y., and Chen, H.C. (2017). Adducin family proteins possess different nuclear export potentials. J. Biomed. Sci. *24*, 30. https://doi.org/10.1186/s12929-017-0333-0.

17. Boito, R., Menniti, M., Amato, R., Palmieri, C., Marinaro, C., Iuliano, R., Tripodi, G., Cusi, D., Fuiano, G., and Perrotti, N. (2005). RFX-1, a putative alpha Adducin interacting protein in a human kidney library. FEBS Lett. *579*, 6439–6443. https://doi.org/10.1016/j.febslet.2005.10.040.

18. de Pater, E., and Trompouki, E. (2018). Bloody Zebrafish: Novel Methods in Normal and Malignant Hematopoiesis. Front. Cell Dev. Biol. *6*, 124. https://doi.org/10.3389/fcell.2018.00124.

19. Ellett, F., and Lieschke, G.J. (2010). Zebrafish as a model for vertebrate hematopoiesis. Curr. Opin. Pharmacol. *10*, 563–570. https://doi.org/10.1016/j.coph.2010.05.004.

20. Han, Y., Mu, Y., Li, X., Xu, P., Tong, J., Liu, Z., Ma, T., Zeng, G., Yang, S., Du, J., and Meng, A. (2011). Grhl2 deficiency impairs otic development and hearing ability in a zebrafish model of the progressive dominant hearing loss DFNA28. Hum. Mol. Genet. *20*, 3213–3226. https://doi.org/10.1093/hmg/ddr234.

21. Zhao, X., Zhao, L., Tian, T., Zhang, Y., Tong, J., Zheng, X., and Meng, A. (2010). Interruption of cenph causes mitotic failure and embryonic death, and its haploinsufficiency suppresses cancer in zebrafish. J. Biol. Chem. *285*, 27924–27934. https://doi.org/10.1074/jbc.M110.136077.

22. Kimmel, C.B., Ballard, W.W., Kimmel, S.R., Ullmann, B., and Schilling, T.F. (1995). Stages of embryonic development of the zebrafish. Dev. Dynam. *203*, 253–310. https://doi.org/10.1002/aja.1002030302.

23. Kawakami, K., Takeda, H., Kawakami, N., Kobayashi, M., Matsuda, N., and Mishina, M. (2004). A transposon-mediated gene trap approach identifies developmentally regulated genes in zebrafish. Dev. Cell *7*, 133–144. https://doi.org/10.1016/j.devcel.2004.06.005.

24. Yang, S., Ning, G., Hou, Y., Cao, Y., Xu, J., Wu, J., Zhang, T., and Wang, Q. (2022). Myoneurin regulates BMP signaling by competing with Ppm1a for Smad binding. iScience *25*, 104495. https://doi.org/10.1016/j.isci.2022.104495.

25. Zheng, X., Yang, S., Han, Y., Zhao, X., Zhao, L., Tian, T., Tong, J., Xu, P., Xiong, C., and Meng, A. (2012). Loss of zygotic NUP107 protein causes missing of pharyngeal skeleton and other tissue defects with impaired nuclear pore function in zebrafish embryos. J. Biol. Chem. *287*, 38254–38264. https://doi.org/10.1074/jbc.M112.408997.

26. Amatruda, J.F., and Zon, L.I. (1999). Dissecting hematopoiesis and disease using the zebrafish. Dev. Biol. *216*, 1–15. https://doi.org/10.1006/dbio.1999.9462.

27. Detrich, H.W., 3rd, Kieran, M.W., Chan, F.Y., Barone, L.M., Yee, K., Rundstadler, J.A., Pratt, S., Ransom, D., and Zon, L.I. (1995). Intraembryonic hematopoietic cell migration during vertebrate development. Proc. Natl. Acad. Sci. USA *92*, 10713–10717. https://doi.org/10.1073/pnas.92.23.10713.

28. Matsuoka, Y., Li, X., and Bennett, V. (2000). Adducin: structure, function and regulation. Cell. Mol. Life Sci. *57*, 884–895. https://doi.org/10.1007/PL00000731.

29. Nehls, V., Drenckhahn, D., Joshi, R., and Bennett, V. (1991). Adducin in erythrocyte precursor cells of rats and humans: expression and compartmentalization. Blood *78*, 1692–1696.

30. Zhao, L., Zhao, X., Tian, T., Lu, Q., Skrbo-Larssen, N., Wu, D., Kuang, Z., Zheng, X., Han, Y., Yang, S., et al. (2008). Heart-specific isoform of tropomyosin4 is essential for heartbeat in zebrafish embryos. Cardiovasc. Res. *80*, 200–208. https://doi.org/10.1093/cvr/cvn177.

31. de Jong, J.L.O., and Zon, L.I. (2005). Use of the zebrafish system to study primitive and definitive hematopoiesis. Annu. Rev. Genet. *39*, 481–501. https://doi.org/10.1146/annurev.genet.39.073003.095931.

32. Bresciani, E., Confalonieri, S., Cermenati, S., Cimbro, S., Foglia, E., Beltrame, M., Di Fiore, P.P., and Cotelli, F. (2010). Zebrafish numb and numblike are involved in primitive erythrocyte differentiation. PLoS One *5*, e14296. https://doi.org/10.1371/journal.pone.0014296.

33. Kristó, I., Bajusz, I., Bajusz, C., Borkúti, P., and Vilmos, P. (2016). Actin, actin-binding proteins, and actin-related proteins in the nucleus. Histochem. Cell Biol. *145*, 373–388. https://doi.org/10.1007/s00418-015-1400-9.

34. Sainz de la Maza, D., Hof-Michel, S., Phillimore, L., Bökel, C., and Amoyel, M. (2022). Cell-cycle exit and stem cell differentiation are coupled through regulation of mitochondrial activity in the Drosophila testis. Cell Rep. *39*, 110774. https://doi.org/10.1016/j.celrep.2022.110774.

35. Grant, S., and Dent, P. (2002). Conversion of drug-induced differentiation to apoptosis by pharmacologic cyclin-dependent kinase inhibitors. Cell Cycle *1*, 383–388. https://doi.org/10.4161/cc.1.6.260.

36. Boutelle, A.M., and Attardi, L.D. (2021). p53 and Tumor Suppression: It Takes a Network. Trends Cell Biol. *31*, 298–310. https://doi.org/10.1016/j.tcb.2020.12.011.

37. Anong, W.A., Franco, T., Chu, H., Weis, T.L., Devlin, E.E., Bodine, D.M., An, X., Mohandas, N., and Low, P.S. (2009). Adducin forms a bridge between the erythrocyte membrane and its cytoskeleton and regulates membrane cohesion. Blood *114*, 1904–1912. https://doi.org/10.1182/blood-2009-02-203216.

38. Bielczyk-Maczyńska, E., Lam Hung, L., Ferreira, L., Fleischmann, T., Weis, F., Fernández-Pevida, A., Harvey, S.A., Wali, N., Warren, A.J., Barroso, I., et al. (2015). The Ribosome Biogenesis Protein Nol9 Is Essential for Definitive Hematopoiesis and Pancreas Morphogenesis in Zebrafish. PLoS Genet. *11*, e1005677. https://doi.org/10.1371/journal.pgen.1005677.

39. Taylor, A.M., Macari, E.R., Chan, I.T., Blair, M.C., Doulatov, S., Vo, L.T., Raiser, D.M., Siva, K., Basak, A., Pirouz, M., et al. (2020). Calmodulin inhibitors improve erythropoiesis in Diamond-Blackfan anemia. Sci. Transl. Med. *12*, eabb5831. https://doi.org/10.1126/scitranslmed.abb5831.

40. Imamura, S., Uchiyama, J., Koshimizu, E., Hanai, J.I., Raftopoulou, C., Murphey, R.D., Bayliss, P.E., Imai, Y., Burns, C.E., Masutomi, K., et al. (2008). A non-canonical function of zebrafish telomerase reverse transcriptase is required for developmental hematopoiesis. PLoS One *3*, e3364. https://doi.org/10.1371/journal.pone.0003364.

41. Andolfo, I., Russo, R., Gambale, A., and Iolascon, A. (2016). New insights on hereditary erythrocyte membrane defects. Haematologica *101*, 1284–1294. https://doi.org/10.3324/haematol.2016.142463.

42. Franco, T., and Low, P.S. (2010). Erythrocyte adducin: a structural regulator of the red blood cell membrane. Transfus. Clin. Biol. *17*, 87–94. https://doi.org/10.1016/j.tracli.2010.05.008.

43. Robledo, R.F., Seburn, K.L., Nicholson, A., and Peters, L.L. (2012). Strain-specific hyperkyphosis and megaesophagus in Add1 null mice. Genesis *50*, 882–891. https://doi.org/10.1002/dvg.22342.

44. Robinson, M.D., McCarthy, D.J., and Smyth, G.K. (2010). edgeR: a Bioconductor package for differential expression analysis of digital gene expression data. Bioinformatics *26*, 139–140. https://doi.org/10.1093/bioinformatics/btp616.

45. Yu, G., Wang, L.G., Han, Y., and He, Q.Y. (2012). clusterProfiler: an R package for comparing biological themes among gene clusters. OMICS *16*, 284–287. https://doi.org/10.1089/omi.2011.0118.

STAR★METHODS

KEY RESOURCES TABLE

REAGENT or RESOURCE	SOURCE	IDENTIFIER
Antibodies		
Monoclonal mouse anti-Add1 antibody	Novus	NB110-55442
Rabbit GFP Polyclonal Antibody	Thermo Fisher Scientific	Cat#A-11122
Sheep Anti-Digoxigenin-AP	Roche	Cat# 11093274910
Donkey anti-Rabbit, Alexa Fluor 488	Thermo Fisher Scientific	Cat# A-21206
Donkey anti-Mouse, Alexa Fluor 594	Thermo Fisher Scientific	Cat# A-21125
Chemicals, peptides, and recombinant proteins		
JUNG tissue freezing medium	Leica	NO. 0201 08926
o-dianisidine	Sigma	N/A
RNA Polymerase, T7	Roche	Cat#10881775001
GP-transfect-mate	GenePharma	NO.220901
Critical commercial assays		
RNeasy Mini Kit	Qiagen	N/A
FirstChoice® RLM-RACE Kit	Ambion	N/A
ApopTag® Red *In Situ* Apoptosis Detection Kit	Millipore	S7165
TruSeq® RNA Sample Preparation Kit	Illumina	N/A
Luc-Pair™ Duo-Luciferase Assay Kit 2.0	GeneCpoeia™	Cat#LF-002
Experimental models: Cell lines		
HEK293	ATCC	CRL-1573
Experimental models: Organisms/strains		
Tg (gata1:EGFP)	This paper	N/A
Tg (fli1:EGFP)	This paper	N/A
Tg (c-myb:EGFP)	This paper	N/A
p53^{M214K}	This paper	N/A
Oligonucleotides		
add1-F:	This paper	N/A
5′-TTTAATATTATGATCTACCATGTTGT-3′	This paper	N/A
add1-R:	This paper	N/A
5′-ATAGGAATAAACAATAATAGCAATAA-3′	This paper	N/A
T3-3:	This paper	N/A
5′-CCTAAGTACTTGTACTTTCACTTG-3′	This paper	N/A
add1-qPCR Forward:	This paper	N/A
5′-CGTTCATTTGTCCAGGGGGA -3′	This paper	N/A
add1-qPCR Reverse:	This paper	N/A
5′- GGCTGACCTTCGTCTTCTCC -3′	This paper	N/A
β-actin-qPCR Forward:	This paper	N/A
5′-ACCATCACCAGAGTCCATCACG-3′	This paper	N/A
p53-qPCR Forward:	This paper	N/A
5′-CTTCTTCAGCTACATTACGACCTGAGGGGAGC-3′	This paper	N/A
p53-qPCR Reverse:	This paper	N/A

(*Continued on next page*)

Continued

REAGENT or RESOURCE	SOURCE	IDENTIFIER
5′-GCAGGCACCACATCACTTAACTCCAGACTG-3′	This paper	N/A
mdm2-qPCR Forward:	This paper	N/A
5′-CCTCACAACAGCAGCGCAGGAGGAGGAGAAG-3′	This paper	N/A
mdm2-qPCR Reverse:	This paper	N/A
5′- CAGGCCACCAATCACGCACCAAGACAGGCTG-3′	This paper	N/A
casp8-qPCR Forward:	This paper	N/A
5′- GAGGAATTGTGTCCCAAGAAAG-3′	This paper	N/A
casp8-qPCR Reverse:	This paper	N/A
5′- TCCAACGTGTGTCCAGTCAATC-3′	This paper	N/A
gaddα*a*-qPCR Forward:	This paper	N/A
5′- GAGGAATTGTGTCCCAAGAAAG-3′	This paper	N/A
gaddα*a*-qPCR Reverse:	This paper	N/A
5′- TCCAACGTGTGTCCAGTCAATC-3′	This paper	N/A
p53 MO:	This paper	N/A
5′-GCGCCATTGCTTTGCAAGAATTG-3′	This paper	N/A
add1 MO:	This paper	N/A
5′-TGTGTCACTGTTTGTTTCTGCAAGC-3′	This paper	N/A
Recombinant DNA		
pEZX-FR01-*p53* promoter	GeneCopoeia	N/A
pcDNA3.1(+)-*ADD1*	Promega	N/A
Software and algorithms		
CM1900	Leica	N/A
SteREO Discovery.V20	Zeiss	N/A
H-7650 electron microscope	HITACHI	N/A
Qubit® 2.0 Fluorometer	Life Technologies	N/A
HiSeq Xten	Illumina	N/A
R package clusterProfiler v.3.16	(Yu G, et al. 2012)[45]	(https://bioconductor.org/packages/clusterProfiler/)
Deposited data		
GEO database	GSE236659	N/A

RESOURCE AVAILABILITY

Lead contact

Further information and requests for resources and reagents should be directed to and will be fulfilled by the Lead Contact Shaoguang Sun (sunshaoguang00@163.com (S.S.)).

Materials availability

Plasmids and animal models generated in this paper will be shared freely upon request to the lead contact.

Data and code availability

Data: All data reported in this paper will be shared by the lead contact upon request.

Code: This paper does not report original code.

Any additional information required to reanalyze the data in this paper is available from the lead contact upon request. RNA-seq are deposited in a publicly accessible database, and the accession numbers in the key resources table under Deposited heading.

EXPERIMENTAL MODEL AND STUDY PARTICIPANT DETAILS

Zebrafish strains and transgenesis

WT AB stocks of Danio rerio, the transgenic lines Tg (*gata1*:EGFP), Tg (*fli1*:EGFP), Tg (*c-myb*:EGFP) and *p53* mutant line were raised and maintained under standard laboratory conditions at 28.5°C. The transposon vector TSG was constructed as previously described.[20] At the one-cell stage, 50 ng of TSG plasmid and 100 pg of *tol2* mRNA were coinjected into the embryos. The implanted founder (F0) embryos were grown to adulthood, crossed with WT zebrafish, and their offspring (F1) were examined under a fluorescent microscope to determine the pattern of GFP expression. To create transgenic lines, the GFP-positive transgenic embryos were raised to adulthood. We created the transgenic zebrafish line $add1^{+/-}$ for this pilot study.

Embryo stages were determined by morphology as previously described.[22]

Ethical approval

All zebrafish experiments were in strict accordance with the Regulations for the Care and Use of Laboratory Animals as published by the Ministry of Science and Technology of China, and the Institute of Zoology's Guidelines for the Care and Use of Laboratory Animals.

METHOD DETAILS

5′-RACE analysis

Total RNAs were isolated from 50 GFP-positive embryos at 24 hpf using RNeasy Mini Kit (Qiagen, CA), and cDNA amplification was performed using FirstChoice RLM-RACE Kit (Ambion) according to the manufacturer's instructions.

Genotyping and quantitative real-time PCR

Embryos from $add1^{+/-}$ intercrosses were divided into three classes for genotyping based on the level of fluorescence at 24 hpf. The main resources table lists three specific primers *add1*-F, *add1*-R, and T3-3 that were utilized for a genotyping experiment with genomic DNA isolated from a single embryo.

Total RNAs from siblings and $add1^{-/-}$ embryos were collected from a pool of 30 embryos at the appropriate stages using the RNeasy Mini Kit (Qiagen, 74104) for quantitative real-time PCR (qRT-PCR). Following the manufacturer's instructions (TOYOBO, TRT-101) qRT-PCR was performed using TB Green Premix Ex TaqTM II (Takara, RR820A) in the Mx3000P real-time PCR system (Stratagene). cDNAs were created from 2 μg of RNA using oligo-dT primer. Actin expression levels were examined as an internal control.

The primer sequences for qRT-PCR were shown in key resources table.

Morpholino, mRNA, and plasmid microinjection

Add1 MO was designed to target the translational start region of zebrafish *add1* and was purchased from Gene Tools LLC. *p53* MO was purchased from Gene Tools LLC. Morpholino or mRNA were injected into the yolk, while plasmid DNA was injected into the cytoplasm of one-cell stage embryos.

Cryosectioning and *o*-dianisidine staining

Embryos stained with phalloidine were embedded using JUNG tissue freezing medium (Leica, order NO. 0201 08926) and snap-frozen in liquid nitrogen. Sagittal sections of embryos were cut in 20 μm thickness by Leica CM1900. Sections were transferred onto slides and stored at −20°C for confocal observation. For the staining of globin, live anesthetized embryos were stained with *o*-dianisidine staining solution (40% anhydrous ethanol, 0.65% hydrogen peroxide, 10 mM sodium acetate, and 0.6 mg/mL *o*-dianisidine (Sigma) in the dark for 15 min as described previously.[25]

Whole-mount *in situ* hybridization and immunostaining

Digoxigenin-UTP-labeled RNA probes for *add1*, *add2*, *add3*, *gata1*, *runx1*, *hbαe3*, and *hbβe1*, *mdm2*, *p53*, *casp8*, *gaddαa* were synthesized *in vitro* from linearized DNA templates using the RNA Polymerase, T7

system (Roche, Cat#10881775001) and according to the manufacturer's instructions. WISH were performed following the standard procedure.

Embryos preserved in 4% paraformaldehyde were dehydrated for at least 2 h in graded methanol and stored at −20°C before being rehydrated three times for 5 min each in PBST (1 × PBS, 0.1% Triton X-100). The embryos were heated in a microwave for 10 min at 94°C–100°C while being immersed in 1 mM EDTA (pH 8.0) to repair antigens. After being washed three times with PBST, the embryos were incubated for an hour at room temperature in block solution (5% fetal calf serum, 1% dimethyl sulfoxide, and 2% BSA in PBST). A 1:1000 concentration of monoclonal mouse anti-Add1 antibody (Novus, NB110-55442) was added, and the embryos were then incubated at 4°C overnight before being washed three times with PBST for 15 min each. After that, embryos were incubated for 4 h at 4°C with DAPI (1:10,000, Sigma) and goat anti-mouse IgG dyed with DyLight 594 (1:500, 715-585-150, Jackson). The embryos were then photographed with a Nikon A1R$^+$ confocal microscope after being put in 1% low melting point agarose.

TUNEL assay

For detection of apoptotic cells in embryos, TUNEL assay was performed using ApopTag Red *In Situ* Apoptosis Detection Kit (Millipore, S7165) according to the manufacturer's instruction with some modifications. The stained embryos were mounted in 1% low melting point agarose and imaged using a laser scanning confocal microscope (Zeiss LSM780).

Transmission electron microscopy

Zebrafish embryos at desired stages were fixed by 2.5% glutaraldehyde (pH7.2) overnight at 4°C, osmicated in 1% osmium tetroxide (OsO4), and dehydrated with graded cold ethanol in series acetone. Next, the embryos were embedded in the Spur resin and polymerized for 2 days. The heart and blood island regions were cut sagittally. Sections were stained with lead citrate and imaged under a HITACHI H-7650 electron microscope.

Cell sorting and RNA sequencing

The trunk region of 50–80 embryos from *add1*:Tg (*gata1*:EGFP) mutants and siblings at 22 hpf were dissected separately and dissociated into single cells with trypsin. GFP$^+$ cells were sorted using BD FACS Aria I. Total RNAs were isolated using SMART-Seq HT Kit. Paired-end libraries were synthesized by using the TruSeq RNA Sample Preparation Kit (Illumina, USA). Using reverse transcriptase and random primers, the cleaved RNA fragments were converted into first-strand cDNA. The second strand of cDNA was then synthesized using DNA Polymerase I and RNase H. These cDNA fragments were then subjected to an end repair process, the Addition of a single 'A' base, and adapter ligation. To create the final cDNA library, the products were purified and enriched with PCR. To confirm the insert size and calculate the mole concentration, purified libraries were quantified using a Qubit 2.0 Fluorometer (Life Technologies, USA) and validated using an Agilent 2100 bioanalyzer (Agilent Technologies, USA). cBot generated clusters with a library diluted to 10 p.m., which were then sequenced on the Illumina HiSeq Xten (Illumina, USA). The library construction and sequencing were performed at Shanghai Biotechnology Corporation.

Dual-luciferase reporter gene assay

The *p53* promoter was amplified using PCR, and inserted into the luciferase reporter gene vector pEZX-FR01 (GeneCopoeia) at *Spe* I/*BamH* I sites. The pEZX-FR01-*p53* promoter was co-transfected with pcDNA3.1(+)-*ADD1* vector into 293A cells using GPtransfect-Mate (GenePharma, Shanghai, China). Twenty-four hours after co-transfection, the Dual-Luciferase Reporter Assay System (Promega) was performed to measure the luciferase activity based on the manufacturer's instructions. For each analysis, the Renilla luciferase signal was normalized with the firefly luciferase signal.

Data analysis for gene expression

We performed differential expression analysis using R package edgeR v.3.3[44] with parameter bcv (biological coeffient of variation) equals 0.1 based on fragments per kilobase of exon model per million mapped fragments (FPKM) normalized expression data. The genes with $|\log_2\text{FoldChange}| > 1$ and $p < 0.05$ were defined differentially expressed genes (DGE). Functional enrichment analysis was performed using R package clusterProfiler v.3.16.[45] The terms with $p < 0.05$ were considered significantly enriched.

QUANTIFICATION AND STATISTICAL ANALYSIS

The statistical analysis was conducted using GraphPad Prism 9.0 software (GraphPad Software, San Diego, CA, USA). To assess the significance between or within groups, One-way ANOVA or Student's t-tests were utilized. Statistical differences are considered significant at a $p < 0.05$ significance level and marked with "*", very significant at $p < 0.01$ and labeled with "**", and extremely significant at $p < 0.001$ and labeled with "***".